Nonlinear Dyn (2010) 62: 333–347
DOI 10.1007/s11071-010-9720-8

ORIGINAL PAPER

Non-linear dynamic analysis of a HSFD mounted gear-bearing system

Cai-Wan Chang-Jian

Received: 1 February 2010 / Accepted: 8 April 2010 / Published online: 29 April 2010

Abstract An investigation is carried out on the systematic analysis of the dynamic behavior of the hybrid squeeze-film damper (HSFD) mounted a gear-bearing system with strongly non-linear oil-film force and gear meshing force in the present study. The dynamic orbits of the system are observed using bifurcation diagrams plotted using the dimensionless unbalance coefficient, damping coefficient and the dimensionless rotating speed ratio as control parameters. The non-dimensional equations of the gear-bearing system are solved using the fourth order Runge-Kutta method. The onset of chaotic motion is identified from the phase diagrams, power spectra, Poincaré maps, bifurcation diagrams, maximum Lyapunov exponents and fractal dimension of the gear-bearing system. The results presented in this study provide some useful insights into the design and development of a gear-bearing system for rotating machinery that operates in highly rotating speed and highly non-linear regimes.

Keywords Hybrid squeeze-film damper (HSFD) · Gear · Bearing · Non-linear

C.-W. Chang-Jian (✉)
Department of Mechanical and Automation Engineering,
I-Shou University, 1, Section 1, Hsueh-Cheng Rd.,
Ta-Hsu Hsiang, Kaohsiung County, Taiwan 840, ROC
e-mail: cwchangjian@mail.isu.edu.tw

Nomenclature

B	bearing parameter $= \frac{6\mu R^2 L^2}{m\delta^3\omega_n}$
c	radial clearance, $c = R - r$
C	damping coefficient of the gear mesh
d	viscous damping of disk
D	$\frac{d}{m\omega_n}$
e	static transmission error and varies as a function of time
f_x, f_y	components of the fluid film force in horizontal and vertical coordinates
F_r, F_t	components of the fluid film force in radial and tangential directions
h	oil-film thickness, $h = \delta(1 + \varepsilon\cos\theta)$
k	stiffness of the retaining springs
K	stiffness coefficient of the gear mesh
k_d	proportional gain of PD controller
k_p	derivative gain of PD controller
L	bearing length
m	masses lumped at the mid-point
m_p	mass of the pinion
m_g	mass of the gear
O_g	center of gravity of the gear
O_p	center of gravity of the pinion
O_b, O_j	geometric center of the bearing and journal
$p(\theta)$	pressure distribution in the fluid film
p_s	pressure of supplying oil
$p_{c,i}$	pressure in the static pressure chamber
$Q_{in,i}$	the volumetric flow rate into oil chamber i ($i = 1$–4) from the controllable orifice
R	inner radius of the bearing housing
r	radius of the journal

r, t radial and tangent coordinates
s speed parameter $= \frac{\omega}{\omega_n}$; $\omega_n = \sqrt{\frac{k}{m}}$
U $\frac{\rho}{\delta}$
x, y, z horizontal, vertical and axial coordinates
x_0, y_0 damper static displacements
x_j, y_j $X_j/c, Y_j/c, j = p, g$
ρ mass eccentricity
ϕ rotational angle ($\phi = \omega t$)
ω rotating speed of the shaft
φ_b angle displacement of line $O_b O_j$ from the x-coordinate (see Fig. 1)
Ω $\dot{\varphi}_b$
δ radial clearance $= R - r$,
θ the angular position along the oil film from line $O_b O_j$ (see Fig. 1)
θ_1 the rotating angle of gear
θ_2 the rotating angle of pinion
μ oil dynamic viscosity
ε_0 $\sqrt{X_0^2 + Y_0^2}$
β distribution angle of static pressure region
$(\cdot), (')$ derivatives with respect to t and ϕ

1 Introduction

HSFD (Hybrid Squeeze-Film Damper) has been well developed and applied in many fields. Squeeze-film damper bearings are actually a special type of journal bearing with its journal mechanically prevented from rotating but free to vibrate within the clearance space. The squeezing action produces hydrodynamic forces in the fluid film. A squeeze-film damper bearing can be designed such that the journal can statically find its own position with in the clearance or be held centrally within the clearance by retaining springs. If the retaining springs are not used, the influence of contact and wear at zero speed will occur and it will add to the complexity of analysis of squeeze-film damper bearing. In a squeeze-film damper bearing-rotor system, the fluid support pressure is generated entirely by the motion of the journal and depends on the viscosity of the lubricating fluid. However, the hydrodynamic pressure around the bearing is non-linear. It may cause fairly large vibrations of the rotor complicating the analysis of this system.

Holmes et al. [1] published a paper dealing with aperiodic behavior in journal bearings and what may very well have been the first paper about aperiodic behavior in journal bearing systems. Nikolajsent and Holmes [2] reported their observation of nonsynchronous vibrations in a test rig of a flexible, symmetric rotor on two identical plain journal bearings supported by centralized squeeze-film dampers. Sykes and Holmes [3] showed experimental observations of subharmonic motion in squeeze-film bearings and linked this to possible precursors of chaotic motion. At the same time, Kim and Noah [4] analyzed the bifurcation of a modified Jeffcott rotor with bearing clearance. Ehrich [5] used a simple numerical model of a Jeffcott rotor mounted on a non-linear spring. It was found that the vibratory response in the transition zone midway between adjacent zones of subharmonic response has all the characteristics of chaotic behavior. Zhao et al. [6] discussed the subharmonic and quasi-periodic motions of an eccentric squeeze-film damper mounted rigid rotor system. Brown [7] studied a simple model of a rigid and hydrodynamically supported journal bearing, using a short bearing theory. Theoretical and experimental investigations were reported by Adiletta et al. [8–10] in which a rigid rotor in short bearings would have subharmonic, quasi-periodic and chaotic motion for suitable values of the system parameters. Sundararajan and Noah [11] proposed a simple shooting scheme along with an arc-length continuation algorithm with applications to periodically forced rotor systems. The occurrence of periodic, quasi-periodic and chaotic motions was predicted for various ranges of rotor speeds. Chang-Jian and Chen [12–16] presented a series of papers discussing about flexible rotor supported by journal bearings under non-linear suspension and also combined with rub-impact effect, turbulent effect and micropolar lubricant into consideration. They found very bountiful non-periodic responses occurring in rotor-bearing systems and the studies would help engineers or scientists escape undesired motions in either designing or operating rotor-bearing systems.

Although virtually all physical phenomena in the real world can be regarded as non-linear, most of these phenomena can be simplified to a linear form given a sufficiently precise linearization technique. However, this simplification is inappropriate for high-power, high rotating speed gear systems, and its application during the design and analysis stage may result in a flawed or potentially dangerous operation. As a result, non-linear analysis methods are generally preferred within engineering and academic circles. The

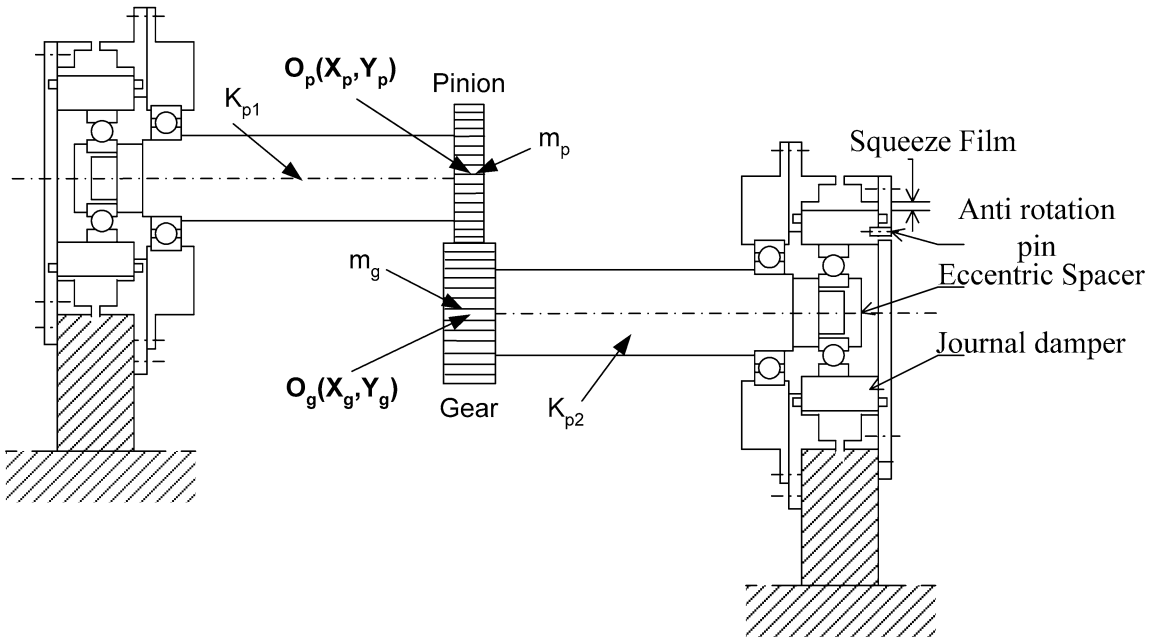

Fig. 1 Schematic illustration of hybrid squeeze-film damper mounted gear-bearing system

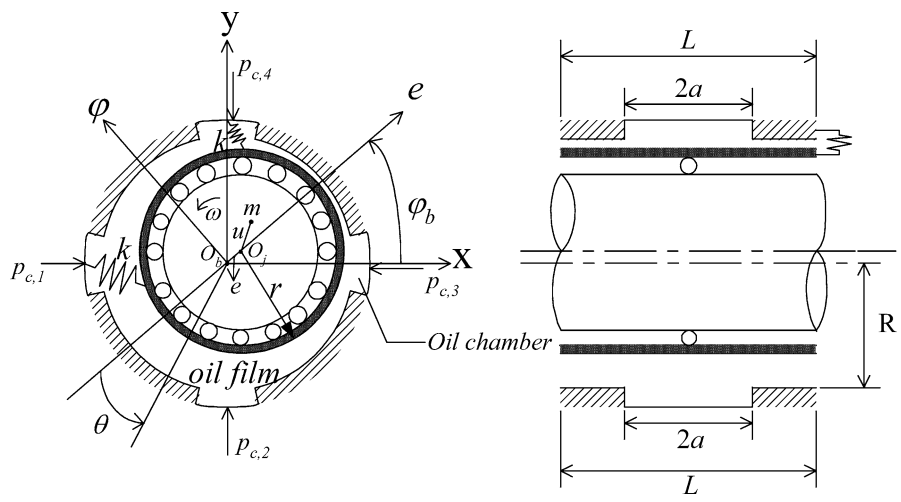

Fig. 2 Cross section of HSFD

current study performs a non-linear analysis of the dynamic behavior of a gear pair system equipped with hybrid squeeze-film damper bearing under gear meshing force effect. The non-dimensional equation of the gear-bearing system is then solved using the fourth order Runge-Kutta method. The non-periodic behavior of this system is characterized using phase diagrams, power spectra, Poincaré maps, bifurcation diagrams, Lyapunov exponents and the fractal dimension of the system.

2 Mathematical modeling

Figure 1 shows a rigid gear pair supported on a hybrid squeeze-film damper (HSFD) in parallel with retaining springs. The bearing consists of four hydrostatic chambers and four hydrodynamic regions. The oil-film supporting force is dependent on the integrated action of hydrodynamic pressure and hydrostatic pressure of HSFD. Figure 2 represents the cross section of HSFD. The structure of this kind bearing should be

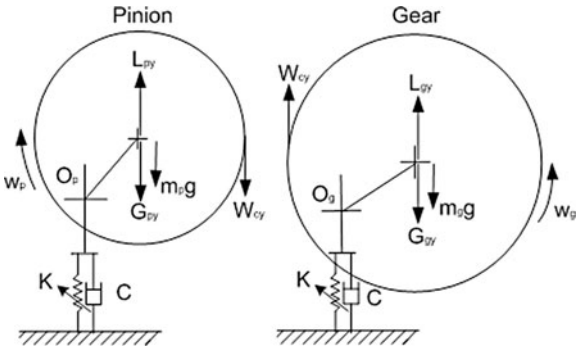

Fig. 3 Model of force diagram for pinion and gear

popularized to consist of $2N$ $(N = 2, 3, 4, \ldots)$ hydrostatic chambers and $2N$ hydrodynamic regions. In this study, oil pressure distribution model in the HSFD is proposed to integrate the pressure distribution of dynamic pressure region and static pressure region as described in Sect. 2.1. Figure 3 presents a schematic illustration of the dynamic model considered between gear and pinion. O_g and O_p are the center of gravity of the gear and pinion, respectively; m_p is the mass of the pinion and m_g is the mass of the gear; K_{p1} and K_{p2} are the stiffness coefficients of the shafts; K is the stiffness coefficient of the gear mesh, C is the damping coefficient of the gear mesh, e is the static transmission error and varies as a function of time.

2.1 The instant oil-film supporting force for HSFD

To analyze the pressure distribution, the Reynolds equation for constant lubricant properties and noncompressibility should be assumed, then the Reynolds equation is as follows [17]

$$\frac{1}{R^2}\frac{\partial}{\partial\theta}\left(h^3\frac{\partial p}{\partial\theta}\right)+\frac{1}{R^2}\frac{\partial}{\partial z}\left(h^3\frac{\partial p}{\partial z}\right) = -12\mu\Omega\frac{\partial h}{\partial\theta}+12\mu\frac{\partial h}{\partial t}. \tag{1}$$

The supporting region of HSFD should be divided into three regions: static pressure region, rotating direction dynamic pressure region and axial direction dynamic pressure region, as shown in Fig. 2. In the part of HSFD with $-a \le z \le a$, the long bearing theory (see Appendix) is assumed and Reynolds equation is solved with the boundary condition of static pressure region $p_{c,i}$ acquiring the pressure distribution $p_0(\theta)$. In the part of HSFD with $a \le |z| \le \frac{L}{2}$, the short bearing theory (see Appendix) is assumed and solves the Reynolds equation with the boundary condition of $p(z,\theta)|_{z=\pm a} = p_0(\theta)$ and $p(z,\theta)|_{z=\pm L/2} = 0$, yielding the pressure distribution in axis direction dynamic pressure region $p(z,\theta)$. Finally, a formula of pressure distribution in whole supporting region is obtained.

According to the above conditions, the instant oil-film pressure distribution is as follows. The instant pressure in rotating direction within the range of $-a \le z \le a$ is

$$p_0(\theta) = \begin{cases} p_{c,i}; & \frac{\pi}{2}(i-1)-\frac{\beta}{2}-\varphi_b \\ & \le\theta\le \frac{\pi}{2}(i-1)+\frac{\beta}{2}-\varphi_b, \\ p_i(\theta); & \frac{\pi}{2}(i-1)+\frac{\beta}{2}-\varphi_b \\ & \le\theta\le \frac{\pi}{2}i-\frac{\beta}{2}-\varphi_b, \end{cases} \tag{2}$$

$i = 1, 2, 3, 4.$

Here

$$\begin{aligned} p_i(\theta) = p_{c,i} &+ \frac{6\mu R^2}{\delta^2}\frac{\dot\varepsilon}{\varepsilon}\left[\frac{1}{(1+\varepsilon\cos\theta)^2}\right. \\ &\left.-\frac{1}{(1+\varepsilon\cos\theta_{i1})^2}\right] \\ &+ c_1\int_{\theta_{i1}}^{\theta}\frac{1}{\delta^3(1+\varepsilon\cos\theta)^3}\,d\theta \\ &-\int_{\theta_{i1}}^{\theta}\frac{12\dot\varphi_b\mu\delta\varepsilon R^2\cos\theta}{\delta^3(1+\varepsilon\cos\theta)^3}\,d\theta, \end{aligned} \tag{3}$$

$i = 1, 2, 3, 4,$

$$\begin{aligned} c_1 = \Bigg(& p_{c,i+1}-p_{c,i} \\ &-\frac{6\mu R^2}{\delta^2}\frac{\dot\varepsilon}{\varepsilon}\left[\frac{1}{(1+\varepsilon\cos\theta_{i2})^2}-\frac{1}{(1+\varepsilon\cos\theta_{i1})^2}\right] \\ &+\int_{\theta_{i1}}^{\theta_{i2}}\frac{12\dot\varphi_b\mu\delta\varepsilon R^2\cos\theta}{\delta(1+\varepsilon\cos\theta)^3}\,d\theta\Bigg)\Bigg/ \\ &\int_{\theta_{i1}}^{\theta_{i2}}\frac{1}{\delta^3(1+\varepsilon\cos\theta)^3}\,d\theta, \end{aligned}$$

$$\theta_{i1} = (i-1)\frac{\pi}{2} + \frac{\beta}{2} - \varphi_b,$$

$$\theta_{i2} = i\frac{\pi}{2} - \frac{\beta}{2} - \varphi_b, \quad i = 1, 2, 3, 4.$$

The instant pressure in the axis direction within the range of $a \le |z| \le \frac{L}{2}$ is

$$p(\theta, z) = \left(\frac{L}{2} - |z|\right)\left\{\left[A_1(\theta)\dot{\varphi}_b\varepsilon + A_2(\theta)\dot{\varepsilon}\right]\left(a - |z|\right) + p_0(\theta)\frac{1}{L/2 - a}\right\}, \tag{4}$$

where

$$A_1(\theta) = \frac{6\mu\delta\sin\theta}{\delta^3(1+\varepsilon\cos\theta)^3};$$

$$A_2(\theta) = \frac{6\mu\delta\cos\theta}{\delta^3(1+\varepsilon\cos\theta)^3}.$$

The instant oil-film forces of the different elements are determined by integrating (2) and (4) over the area of the journal sleeve. In the static pressure region, the forces are

$$F_{rs} = \sum_{i=1}^{4} p_{ci} 2aR\left[\sin\left(\frac{\pi}{2}(i-1) + \frac{\beta}{2} - \varphi_b\right) - \sin\left(\frac{\pi}{2}(i-1) - \frac{\beta}{2} - \varphi_b\right)\right], \tag{5}$$

$$F_{\tau s} = \sum_{i=1}^{4} p_{ci} 2aR\left[\cos\left(\frac{\pi}{2}(i-1) - \frac{\beta}{2} - \varphi_b\right) - \cos\left(\frac{\pi}{2}(i-1) + \frac{\beta}{2} - \varphi_b\right)\right]. \tag{6}$$

In the rotating direction dynamics pressure region, the forces are

$$F_{rc} = \sum_{i=1}^{4}\int_{\theta_{i1}}^{\theta_{i2}} p_i(\theta) R 2a\cos\theta\, d\theta, \tag{7}$$

$$F_{\tau c} = \sum_{i=1}^{4}\int_{\theta_{i1}}^{\theta_{i2}} p_i(\theta) R 2a\sin\theta\, d\theta. \tag{8}$$

In the axial direction dynamic pressure region, the forces are

$$F_{ra} = \int_{-L/2}^{-a} dz\int_0^{2\pi} p(\theta, z) R\cos\theta\, d\theta + \int_{L/2}^{a} dz\int_0^{2\pi} p(\theta, z) R\cos\theta\, d\theta, \tag{9}$$

$$F_{\tau a} = \int_{-L/2}^{-a} dz\int_0^{2\pi} p(\theta, z) R\sin\theta\, d\theta + \int_{L/2}^{a} dz\int_0^{2\pi} p(\theta, z) R\sin\theta\, d\theta. \tag{10}$$

The resulting damper forces in the radial and tangential directions are determined by summing the above supporting forces. It is as follows:

$$F_r = F_{rs} + F_{rc} + F_{ra}, \tag{11}$$

$$F_\tau = F_{\tau s} + F_{\tau c} + F_{\tau a}. \tag{12}$$

2.2 The gear meshing force

L_{py} and L_{gy} are the centrifugal forces in the vertical gear mesh direction for pinion and gear, G_{py} and G_{gy} are the inertia forces in the vertical gear mesh direction for pinion and gear, W_{cx} is the dynamic gear mesh force in the horizontal direction, and W_{cy} is the dynamic gear mesh force in the vertical direction. $L_{py}, L_{gy}, G_{py}, G_{gy}, W_{cx}$ and W_{cy} can be performed as

$$L_{py} = m_p e_p \omega_p^2 \sin\theta_1, \tag{13}$$

$$L_{gy} = m_g e_g \omega_g^2 \sin\theta_2, \tag{14}$$

$$G_{py} = m_p e_p \ddot{\theta}_1 \cos\theta_1, \tag{15}$$

$$G_{gy} = m_g e_g \ddot{\theta}_2 \cos\theta_2, \tag{16}$$

$$W_{cx} = C_m\left(\dot{X}_p - \dot{X}_g - e_p\Omega\sin(\Omega t)\right) + K_m\left(X_p - X_g - e_p\cos(\Omega t)\right), \tag{17}$$

$$W_{cy} = C_m\left(\dot{Y}_p - \dot{Y}_g - e_p\Omega\cos(\Omega t)\right) + K_m\left(Y_p - Y_g - e_p\sin(\Omega t)\right). \tag{18}$$

2.3 Dynamics equation

The equations of motion in the Cartesian coordinates can be written as

$$\begin{aligned} &m_p\ddot{X}_p + C\dot{X}_p + KX_p \\ &\quad = C_m\big(\dot{X}_p - \dot{X}_g - e_p\Omega\sin(\Omega t)\big) \\ &\qquad + K_m\big(X_p - X_g - e_p\cos(\Omega t)\big) \\ &\qquad + F_{x1} + KX_{p0}, \end{aligned} \tag{19}$$

$$\begin{aligned} &m_p\ddot{Y}_p + C\dot{Y}_p + KY_p \\ &\quad = m_p e_p\omega_p^2\sin\theta_1 - C_m\big(\dot{Y}_p - \dot{Y}_g - e_p\Omega\cos(\Omega t)\big) \\ &\qquad - K_m\big(Y_p - Y_g - e_p\sin(\Omega t)\big) \\ &\qquad - m_p g + F_{y1} + KY_{p0}, \end{aligned} \tag{20}$$

$$\begin{aligned} &m_g\ddot{X}_g + C\dot{X}_g + KX_g \\ &\quad = -C_m\big(\dot{X}_p - \dot{X}_g - e_p\Omega\sin(\Omega t)\big) \\ &\qquad - K_m\big(X_p - X_g - e_p\cos(\Omega t)\big) \\ &\qquad + F_{x2} + KX_{g0}, \end{aligned} \tag{21}$$

$$\begin{aligned} &m_g\ddot{Y}_g + C\dot{Y}_g + KY_g \\ &\quad = m_g e_g\omega_g^2\sin\theta_2 - C_m\big(\dot{Y}_p - \dot{Y}_g - e_p\Omega\cos(\Omega t)\big) \\ &\qquad + K_m\big(Y_p - Y_g - e_p\sin(\Omega t)\big) \\ &\qquad - m_g g + F_{y2} + KY_{g0}. \end{aligned} \tag{22}$$

The origin of the o–xyz-coordinate system is taken to be the bearing center O_b. Dividing these two equations by $mc\omega^2$ and defining a non-dimensional time $\phi = \omega t$ and a speed parameter $s = \frac{\omega}{\omega_n}$, one obtains the following non-dimensionalized equations of motion:

$$\begin{aligned} x_p'' &= -\frac{2\xi_2}{s}x_p' - \frac{1}{s^2}(x_p - x_1 - \varepsilon_1\cos\varphi_1) \\ &\quad + \beta\cos(\phi/4) - \frac{2\xi_3}{s}\big(x_p' - x_g' - E_p\sin\phi\big) \\ &\quad - \frac{\Lambda}{s^2}(x_p - x_g - E_p\cos\phi) \\ &\quad + \frac{B}{s}\left(\frac{x_pF_r - y_pF_\tau}{\varepsilon}\right) + \frac{x_{p0}}{s^2}, \end{aligned} \tag{23}$$

$$\begin{aligned} y_p'' &= -\frac{2\xi_2}{s}y_p' - \frac{1}{s^2}(y_p - y_1 - \varepsilon_1\sin\varphi_1) \\ &\quad + \beta\sin(\phi/4) - \frac{2\xi_3}{s}\big(y_p' - y_g' - E_p\cos\phi\big) \\ &\quad - \frac{\Lambda}{s^2}(y_p - y_g - E_p\sin\phi) \\ &\quad - \frac{f}{s^2} + \frac{B}{s}\left(\frac{y_pF_r + x_pF_\tau}{\varepsilon}\right) + \frac{y_{p0}}{s^2}, \end{aligned} \tag{24}$$

$$\begin{aligned} x_g'' &= -\frac{2\xi_4}{s}x_g' - \frac{1}{s^2}(x_g - x_2 - \varepsilon_2\cos\varphi_2) \\ &\quad + \beta_g\cos(\phi/8) + \frac{2\xi_5}{s}\big(x_p' - x_g' - E_p\sin\phi\big) \\ &\quad - \frac{\Lambda_g}{s^2}(x_p - x_g - E_p\cos\phi) \\ &\quad + \frac{B}{s}\left(\frac{x_gF_r - y_gF_\tau}{\varepsilon}\right) + \frac{x_{g0}}{s^2}, \end{aligned} \tag{25}$$

$$\begin{aligned} y_g'' &= -\frac{2\xi_4}{s}y_g' - \frac{1}{s^2}(y_g - y_2 - \varepsilon_2\sin\varphi_2) \\ &\quad + \beta_g\sin(\phi/8) + \frac{2\xi_5}{s}\big(y_p' - y_g' - E_p\cos\phi\big) \\ &\quad + \frac{\Lambda_g}{s^2}(y_p - y_g - E_p\sin\phi) \\ &\quad - \frac{f_g}{s^2} + \frac{B}{s}\left(\frac{y_gF_r + x_gF_\tau}{\varepsilon}\right) + \frac{y_{g0}}{s^2}. \end{aligned} \tag{26}$$

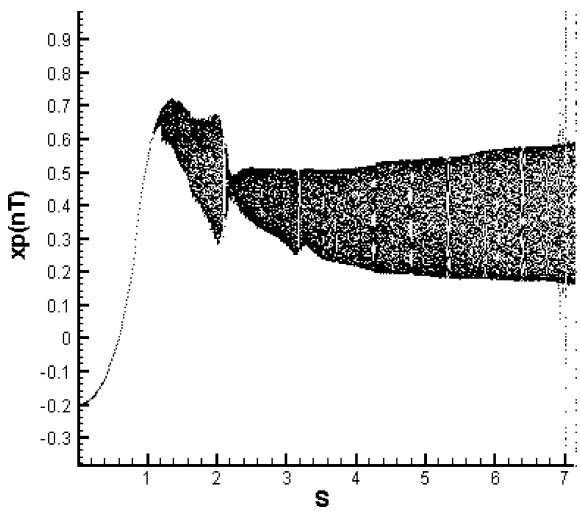

Fig. 4 Bifurcation diagrams of gear-bearing system using dimensionless rotating speed ratio, s, as bifurcation parameter

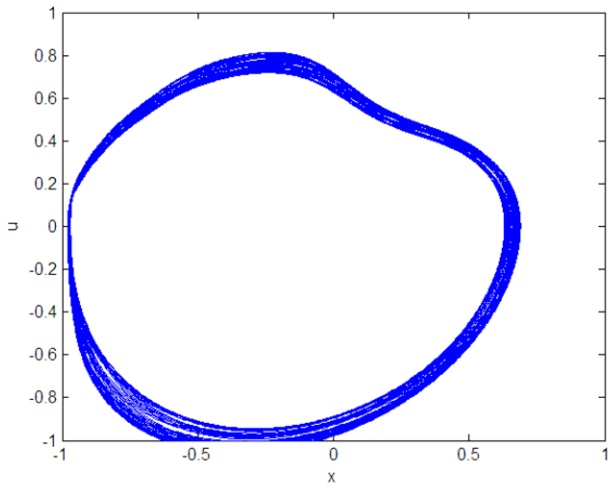

Phase Diagram

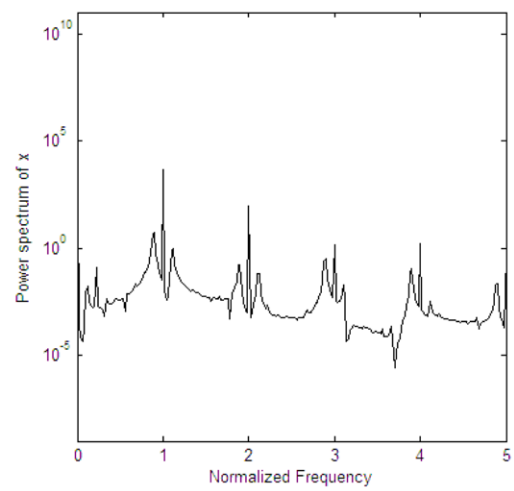

Power Spectrum

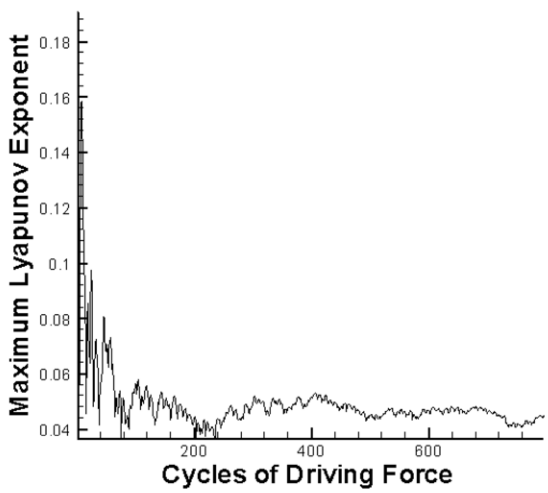

Lyapunov Exponent

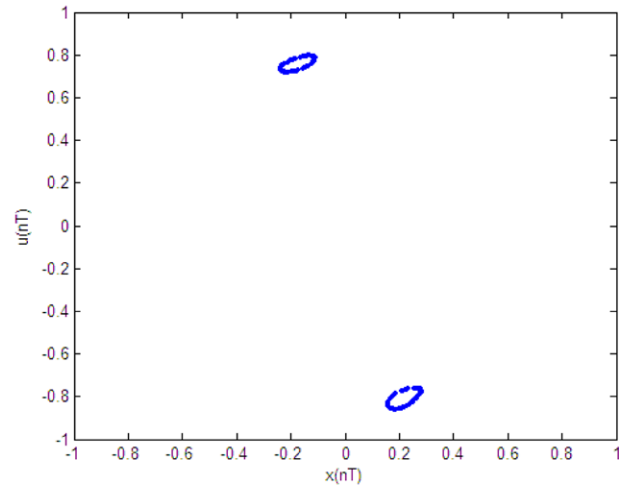

Poincaré Map

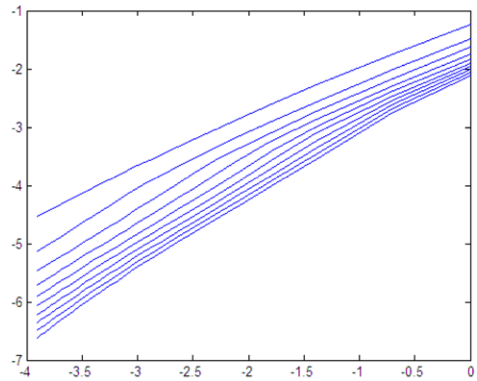

Fractal Dimension

Fig. 5 Simulation results obtained for gear-bearing system with $s = 1.2$ (x_p)

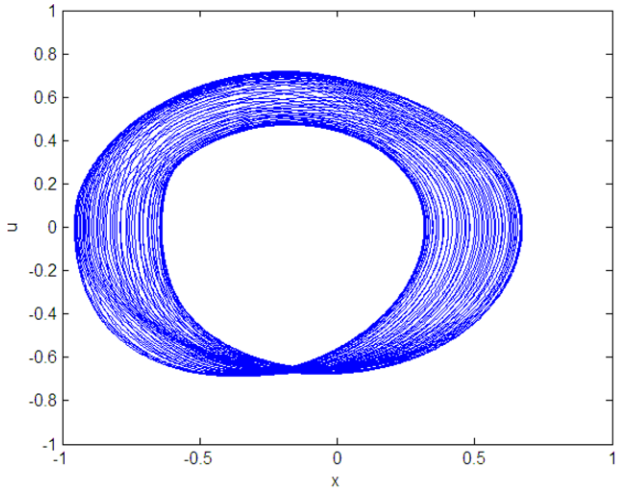

Phase Diagram

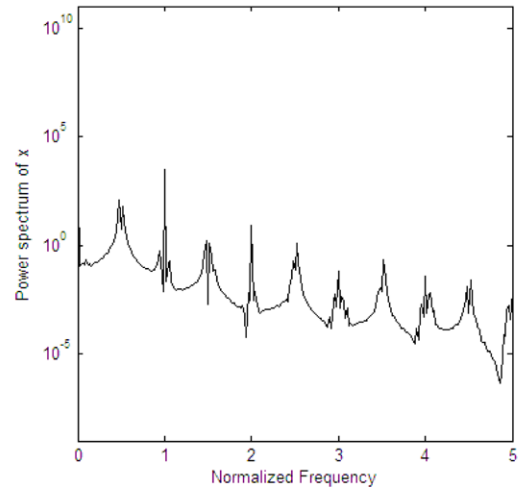

Power Spectrum

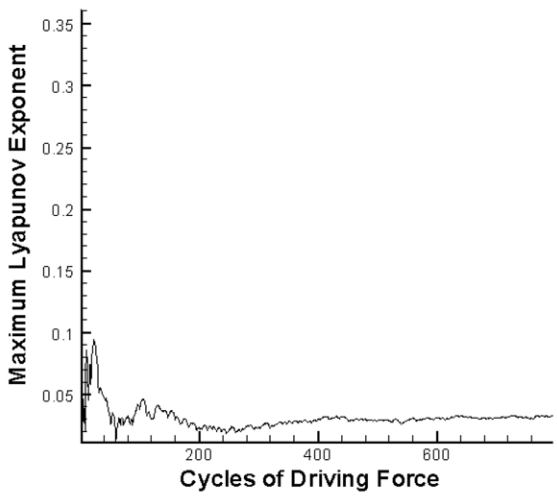

Lyapunov Exponent

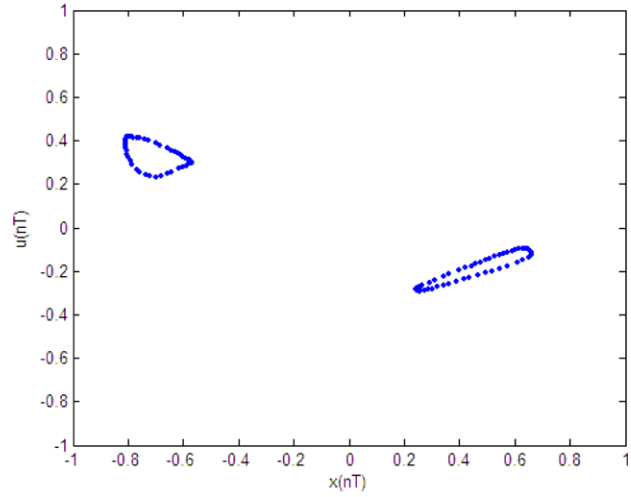

Poincaré Map

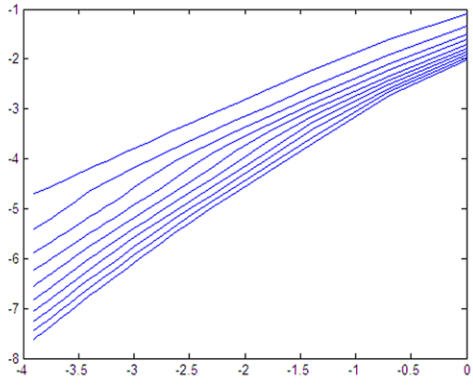

Fractal Dimension

Fig. 6 Simulation results obtained for gear-bearing system with $s = 2.0$ (x_p)

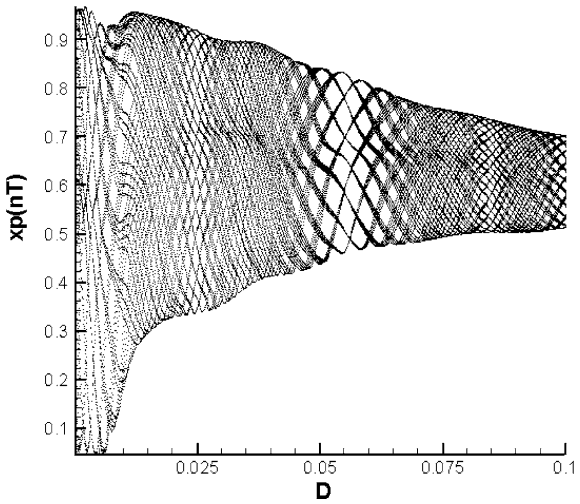

Fig. 7 Bifurcation diagrams of gear-bearing system using dimensionless damping coefficient, D, as bifurcation parameter

Equations (23)–(26) describe a non-linear dynamic system. In the current study, the approximate solutions of these coupled non-linear differential equations are obtained using the fourth order Runge-Kutta numerical scheme.

3 Numerical results and discussions

In the simulations, the system parameters are assigned the following values: $B = 0.3$, $\beta = 0.35$, $\beta_g = 0.35$, $f = 0.2$, $f_g = 0.2$, $\xi_1 = 0.01$, $\xi_2 = 0.02$, $\xi_3 = 0.015$, $\xi_4 = 0.02$, $\xi_5 = 0.015$, $C_{1p} = 2.0$, $\Lambda = 0.04$, $\Lambda_g = 0.04$, $\varepsilon_1 = 0.3$, $\varepsilon_2 = 0.3$ [18].

The non-linear dynamic equations presented in (23) to (26) for the gear-bearing system with strongly non-linear oil-film force and gear meshing force were solved using the fourth order Runge-Kutta method. The time step in the iterative solution procedure was assigned a value of $\pi/300$ and the termination criterion was specified as an error tolerance of less than 0.0001. The time series data corresponding to the first 800 revolutions of the two gears were deliberately excluded from the dynamic analysis to ensure that the analyzed data related to steady-state conditions. The sampled data were used to generate the dynamic trajectories, Poincaré maps and bifurcation diagrams of the spur gear system in order to obtain a basic understanding of its dynamic behavior. The maximum Lyapunov exponent and the fractal dimension measure were then used to identify the onset of chaotic motion. For convenience, only the data of the displacements in the horizontal direction were used to generate diagrams.

The rotating speed ratio s is one of the most significant and commonly used as a control parameter in analyzing dynamic characteristics of bearing systems. Accordingly, the dynamic behavior of the current gear-bearing system was examined using the dimensionless rotating speed ratio s as a bifurcation control parameter. Figure 4 shows the bifurcation diagrams for the gear-bearing system displacement against the dimensionless rotating speed ratio. The bifurcation diagrams show that the geometric center of gear in the horizontal direction performs synchronous $1T$-periodic motion at low values of the rotating speed ratio, i.e. $s < 1.10$ and then the non-periodic motion or the so-called chaotic motion can be found as the dimensionless rotating speed ratio is increased over $s = 1.10$ for pinion center. It can be seen that vibration amplitude is larger for higher rotating speed than low rotating speed. With the increase of rotating speed, dynamic characteristics are disorder and behave non-periodic or even chaotic responses. To illustrate the non-periodic motions more clearly, phase diagrams, power spectra, Poincaré maps, Lyapunov exponents and the fractal dimension are applied to identify the onset of chaotic motions. Figures 5 and 6 represent phase diagrams, power spectra, Poincaré maps, Lyapunov exponents and the fractal dimensions of pinion center with $s = 1.2$ and $s = 2.0$ respectively. The simulation results show that phase diagrams show disordered dynamic behaviors; power spectra reveal numerous excitation frequencies; the return points in the Poincaré maps form geometrically fractal structures; the maximum Lyapunov exponent is positive; the fractal dimensions are found to be 1.16 for x_p at $s = 1.2$ and 1.41 for x_p at $s = 2.0$.

The damping coefficient is also an important control parameter in measuring dynamic responses of vibrating systems. In physical viewpoint, the existence of damping coefficient in vibrating systems make them getting into dissipation systems. Figure 7 is the bifurcation diagram of gear-bearing system using dimensionless damping coefficient, D, as bifurcation parameter at $s = 1.50$. Comparing with the above section, we know that the dynamic response is non-periodic and chaotic at $s = 1.50$. The dy-

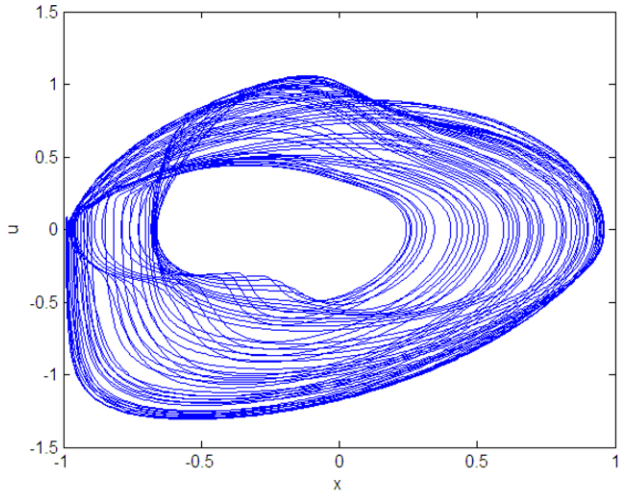

Phase Diagram

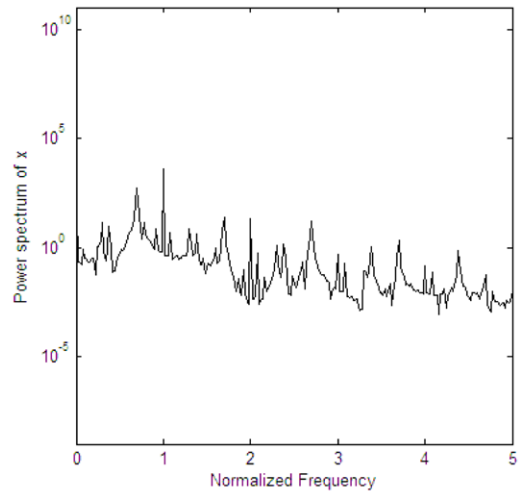

Power Spectrum

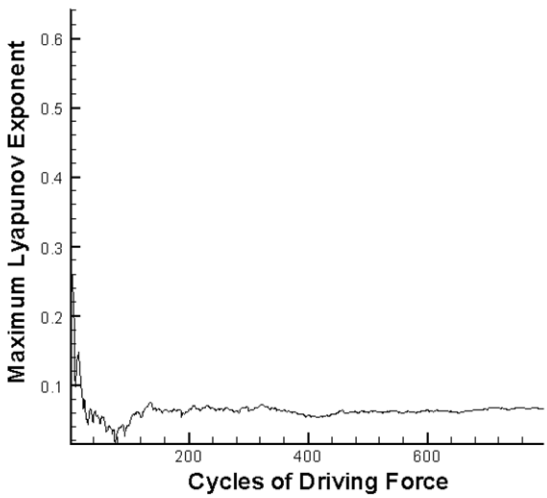

Lyapunov Exponent

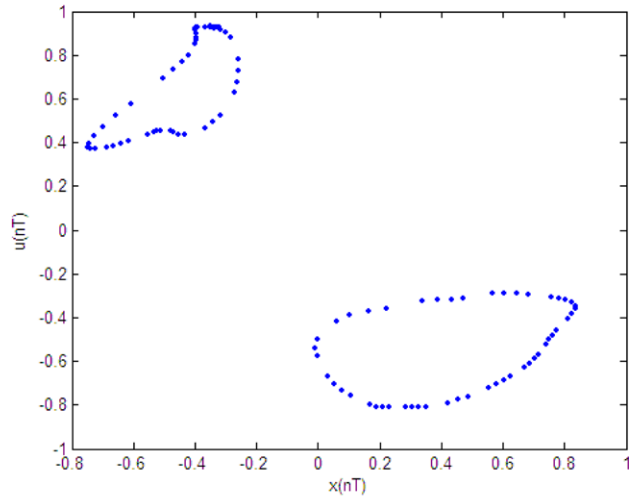

Poincaré Map

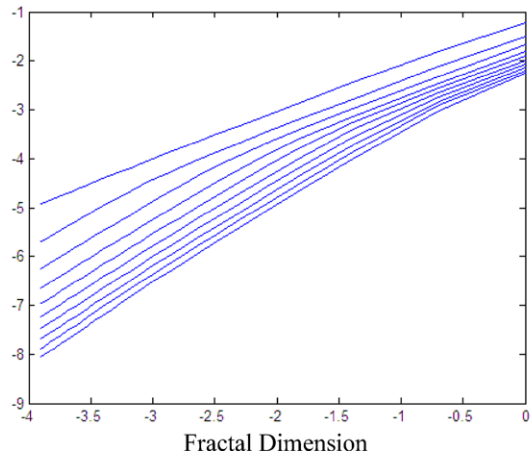

Fractal Dimension

Fig. 8 Simulation results obtained for gear-bearing system with $D = 0.01$ (x_p)

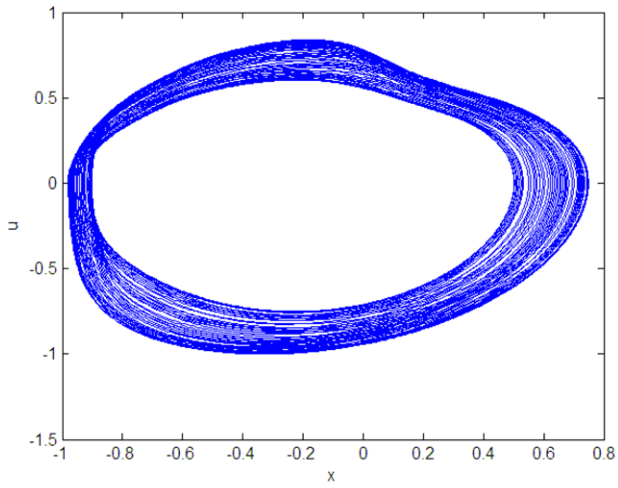

Phase Diagram

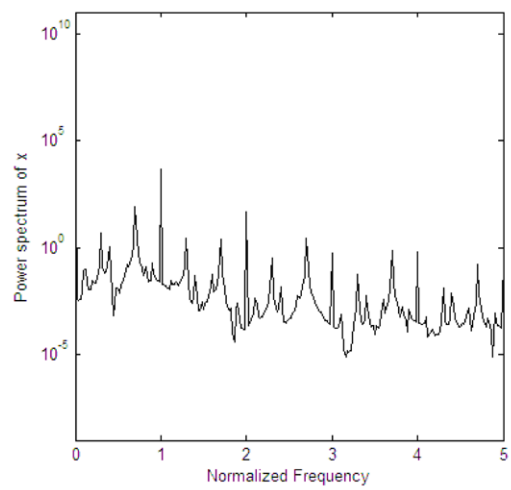

Power Spectrum

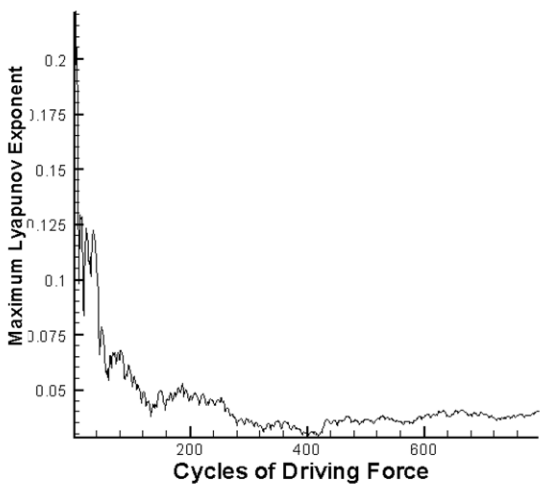

Lyapunov Exponent

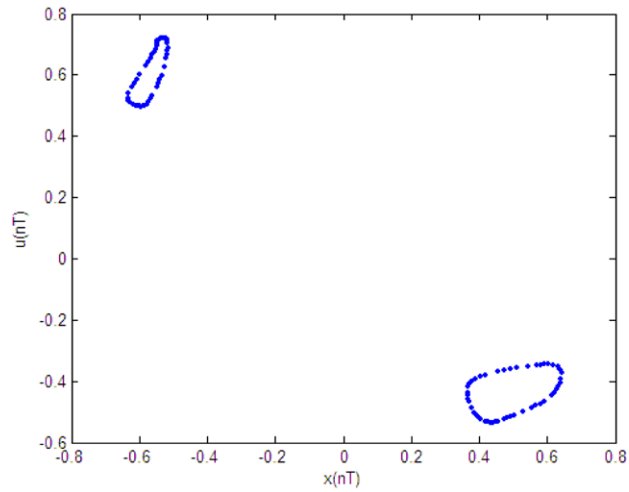

Poincaré Map

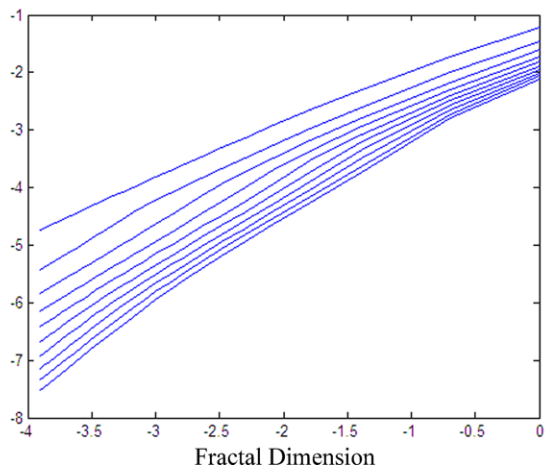

Fractal Dimension

Fig. 9 Simulation results obtained for gear-bearing system with $D = 0.08$ (x_p)

namic characteristics persist disorder and chaotic under all damping coefficients at this rotating speed, i.e. $s = 1.50$. The phase diagrams are shown in Figs. 8 and 9 and they are fully disorder. Besides, power spectra also reveal numerous excitation frequencies and some geometrically fractal structures are also shown in the Poincaré maps. Meanwhile, Lyapunov exponent is positive and the fractal dimensions are found to be 1.43 for x_p at $D = 0.01$ and 1.32 for x_p at $D = 0.08$. The vibration amplitude becomes smaller with the increase of damping coefficient and we can find that damping may not suppress non-periodic motions or disorder motions any more at $s = 1.50$. Therefore, the existence of damping coefficient has some effects in dynamic characteristics of the system.

The unbalance coefficient also plays an important role in controlling dynamic responses in many rotating machineries. Therefore, it is valuable to investigate various dynamic characteristics of the systems for diagnosing some dynamic characteristics and faults by using unbalance parameter as a control parameter. Figure 10 represents the bifurcation diagram of gear center using dimensionless unbalance coefficient, β, as bifurcation parameter. It can be found that system responses exhibit periodic motions at the interval of $0.001 \leq \beta \leq 0.0239$, but display strongly non-periodic motions when $\beta > 0.0239$. Unlike the usual ways into chaos ($1T \Rightarrow 2T \Rightarrow 4T \Rightarrow 8T \Rightarrow 16T \Rightarrow 32T \Rightarrow \cdots \Rightarrow$ chaos or periodic $\Rightarrow$ quasi-periodic $\Rightarrow$ chaotic), it suddenly gets in chaos from the periodic motion without any transition. In Figs. 11 and 12, the irregular and disorder dynamic orbits have shown in phase diagrams and this also reveals that periodic motions do not exist in those situations. Nevertheless, the irregular orbits cannot afford us enough information about what kinds of dynamic response it will be. Therefore, we must use other distinguishing methods to identify dynamic behaviors of the systems under individual situation. The power spectra show numerous excitation frequencies and tell us they are composed of many different frequencies. The Poincaré maps display some geometrically fractal structures (not a single point or a closed curve). The maximum Lyapunov exponent is positive and the fractal dimensions are found to be 1.39 for x_p at $\beta = 0.54$ and 1.36 for x_p at $\beta = 0.55$.

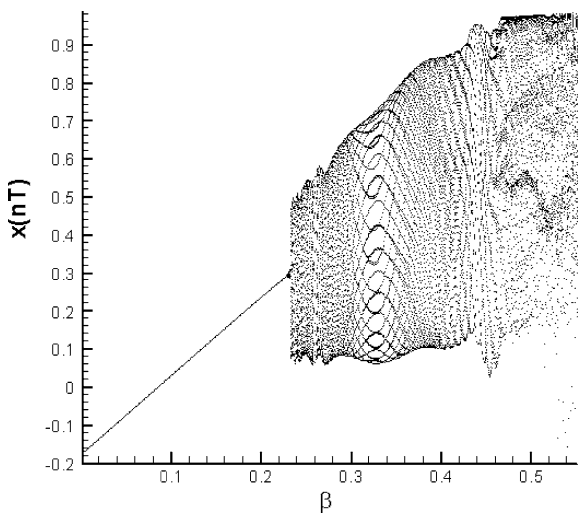

Fig. 10 Bifurcation diagrams of gear-bearing system using dimensionless unbalance coefficient, β, as bifurcation parameter

4 Conclusions

A Hybrid Squeeze-Film Damper Mounted Gear-bearing System with non-linear oil-film force and gear meshing force has been presented and studied by a numerical analysis of the non-linear dynamic response in this study. The dynamics of the system have been analyzed by reference to its dynamic trajectories, power spectra, Poincaré maps, bifurcation diagrams, maximum Lyapunov exponents and fractal dimensions. The effects of the change in the rotating speed ratios, unbalance parameters and damping coefficients on the dynamic characteristics of the gear-bearing system are studied theoretically in detail. It can be observed that very rich non-periodic and chaotic motions exhibit in this system. The formal usual ways into chaos ($1T \Rightarrow 2T \Rightarrow 4T \Rightarrow 8T \Rightarrow 16T \Rightarrow 32T \Rightarrow \cdots \Rightarrow$ chaos or periodic $\Rightarrow$ quasi-periodic $\Rightarrow$ chaotic) are no more found in this study. Overall, the results presented in this study provide a detailed understanding of the non-linear dynamic response of a gear-bearing system under typical unbalance approximations, rotating speed conditions and damping effects. The results will enable suitable values of the unbalance coefficient, damping coefficient and rotating speed ratio to be specified such that chaotic behavior can be avoided, thus reducing the amplitude of the vibration within the system and extending the system life.

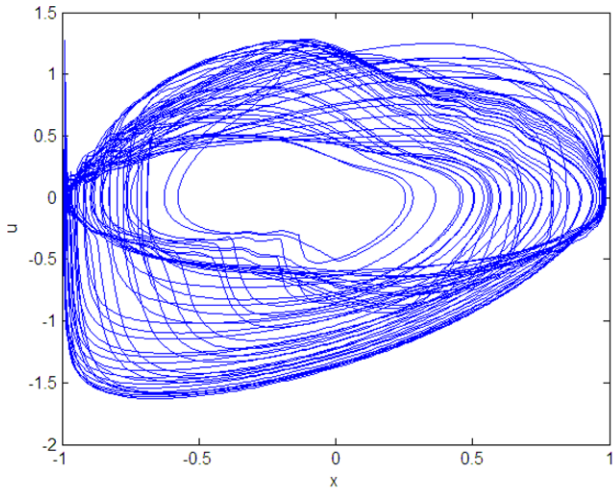

Phase Diagram

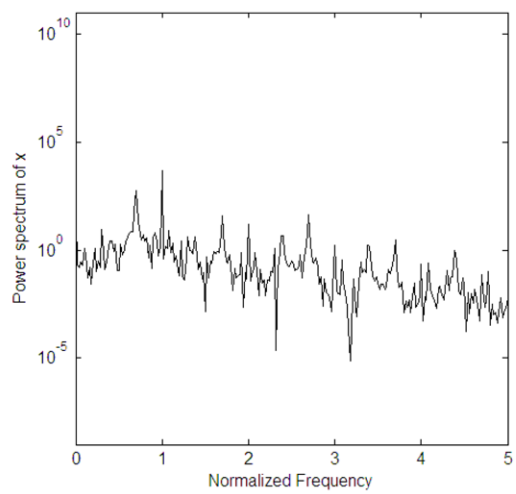

Power Spectrum

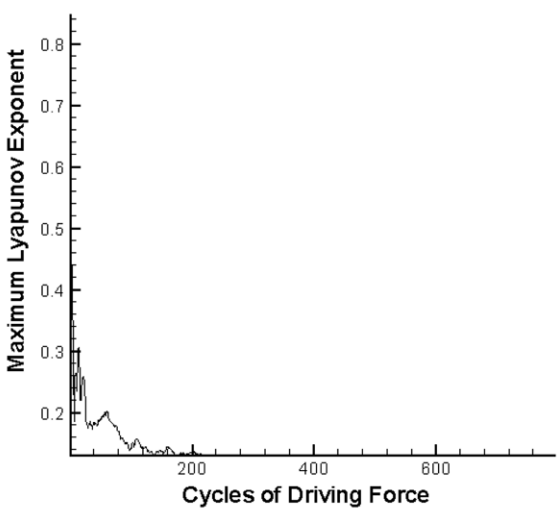

Lyapunov Exponent

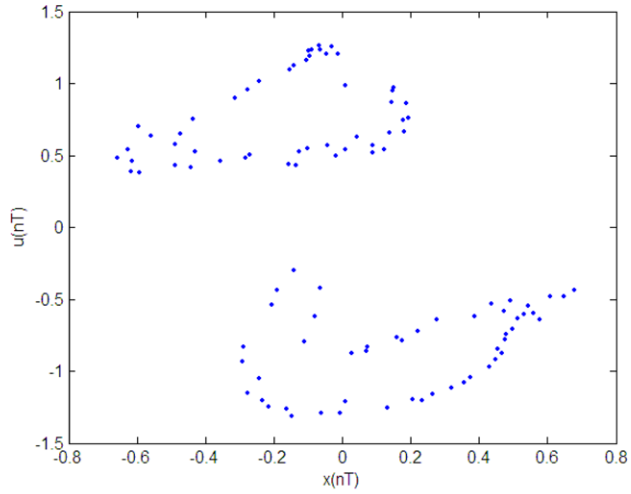

Poincaré Map

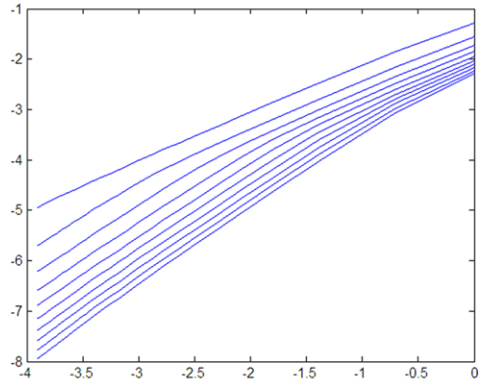

Fractal Dimension

Fig. 11 Simulation results obtained for gear-bearing system with $\beta = 0.54$ (x_p)

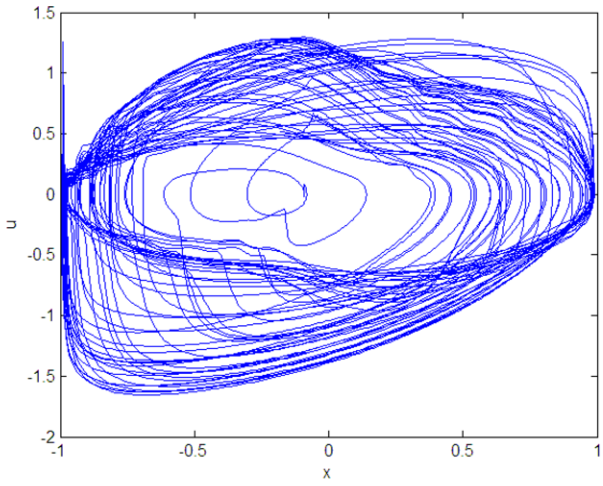

Phase Diagram

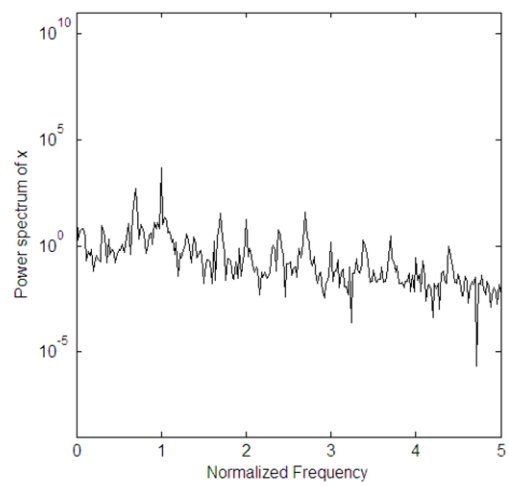

Power Spectrum

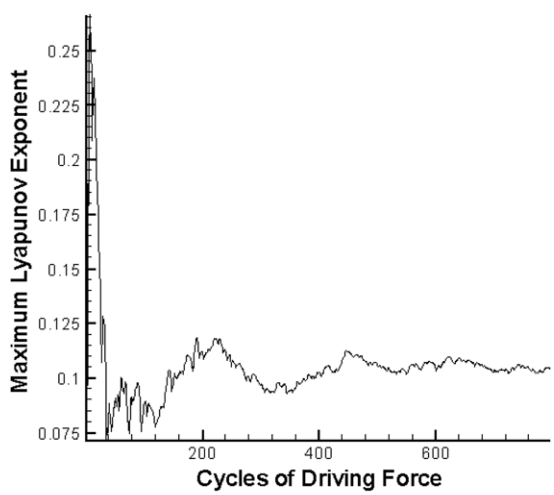

Lyapunov Exponent

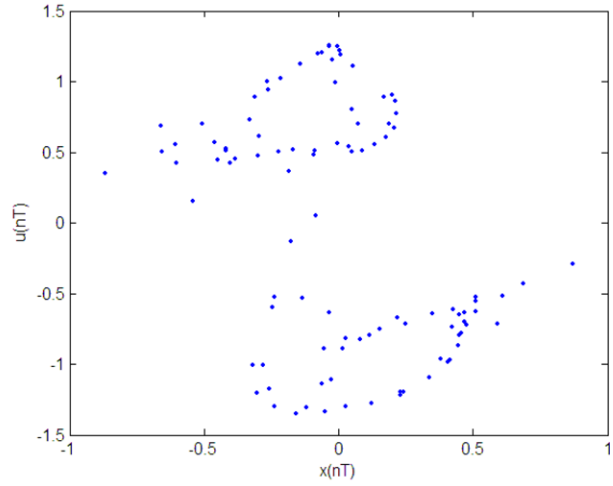

Poincaré Map

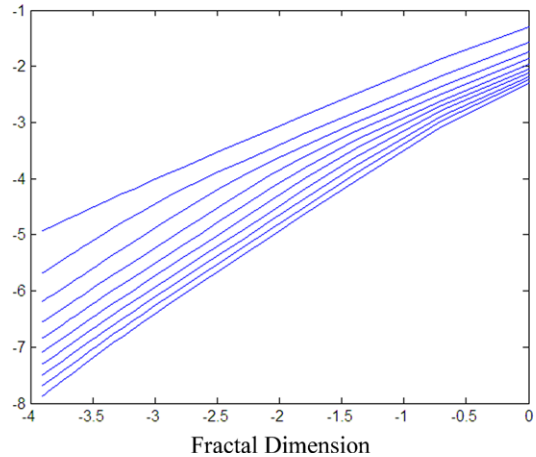

Fractal Dimension

Fig. 12 Simulation results obtained for gear-bearing system with $\beta = 0.55$ (x_p)

Appendix

(1) In the part of HSFD with $-a \le z \le a$, the long bearing theory ($\frac{\partial p}{\partial z} = 0$) is assumed and the traditional Reynolds equation can be modified with $h = c(1 + \varepsilon\cos(\gamma - \varphi_b(t))) = c(1 + \varepsilon\cos\theta)$, $\frac{\partial h}{\partial x} = -\frac{c\varepsilon}{R}\sin\theta$, $\frac{\partial h}{\partial t} = c\dot{\varepsilon}\cos\theta + c\varepsilon\dot{\varphi}_b\sin\theta$, $x = R\theta$, $U = R\omega$, $\varepsilon = \frac{e}{c}$, and then become

$$\frac{1}{R}\frac{\partial}{\partial\theta}\left(\frac{h^3}{\mu}\frac{\partial p}{R\partial\theta}\right) = 12(c\dot{\varepsilon}\cos\theta + c\varepsilon\dot{\varphi}_b\sin\theta). \quad \text{(A.1)}$$

(2) In the part of HSFD with $a \le |z| \le \frac{L}{2}$, the short bearing theory ($\frac{\partial p}{\partial\theta} = 0$) is assumed and the traditional Reynolds equation can be modified with $h = c(1 + \varepsilon\cos(\gamma - \varphi_b(t))) = c(1 + \varepsilon\cos\theta)$, $\frac{\partial h}{\partial x} = -\frac{c\varepsilon}{R}\sin\theta$, $\frac{\partial h}{\partial t} = c\dot{\varepsilon}\cos\theta + c\varepsilon\dot{\varphi}_b\sin\theta$, $x = R\theta$, $U = R\omega$, $\varepsilon = \frac{e}{c}$, and then become

$$\frac{\partial}{\partial z}\left(\frac{h^3}{\mu}\frac{\partial p}{\partial z}\right) = 12(c\dot{\varepsilon}\cos\theta + c\varepsilon\dot{\varphi}_b\sin\theta). \quad \text{(A.2)}$$

References

1. Holmes, A.G., Ettles, C.M., Mayes, I.W.: Aperiodic behavior of a rigid shaft in short journal bearings. Int. J. Numer. Method Eng. **12**, 695–702 (1978)
2. Nikolajsent, J.I., Holmes, R.: Investigation of squeeze-film isolators for the vibration control of a flexible rotor. ASME J. Mech. Sci. **21**(4), 247–252 (1979)
3. Sykes, J.E.H., Holmes, R.: The effect of bearing misalignment on the non-linear vibration of aero-engine rotor-damper assemblies. Proc. Inst. Mech. Eng. **204**, 83–99 (1990)
4. Kim, Y.B., Noah, S.T.: Bifurcation analysis of a modified jeffcot rotor with bearing clearances. Nonlinear Dyn. **1**, 221–241 (1990)
5. Ehrich, F.F.: Some observations of chaotic vibration phenomena in high-speed rotordynamics. ASME J. Vib. Acoust. **113**, 50–57 (1991)
6. Zhao, J.Y., Linnett, I.W., Mclean, L.J.: Subharmonic and quasi-periodic motion of an eccentric squeeze film damper-mounted rigid rotor. ASME J. Vib. Acoust. **116**, 357–363 (1994)
7. Brown, R.D., Addison, P., Chan, A.H.C.: Chaos in the unbalance response of journal bearings. Nonlinear Dyn. **5**, 421–432 (1994)
8. Adiletta, G., Guido, A.R., Rossi, C.: Chaotic motions of a rigid rotor in short journal bearings. Nonlinear Dyn. **10**, 251–269 (1996)
9. Adiletta, G., Guido, A.R., Rossi, C.: Nonlinear dynamics of a rigid unbalanced rotor in short bearings. Part I: Theoretical analysis. Nonlinear Dyn. **14**, 57–87 (1997)
10. Adiletta, G., Guido, A.R., Rossi, C.: Nonlinear dynamics of a rigid unbalanced rotor in short bearings. Part II: Experimental analysis. Nonlinear Dyn. **14**, 157–189 (1997)
11. Sundararajan, P., Noah, S.T.: Dynamics of forced nonlinear systems using shooting/arc-length continuation method—Application to rotor systems. ASME J. Vib. Acoust. **119**, 9–20 (1997)
12. Chang-Jian, C.W., Chen, C.K.: Chaos and bifurcation of a flexible rub-impact rotor supported by oil film bearings with non-linear suspension. Mech. Mach. Theory **42**(3), 312–333 (2007)
13. Chang-Jian, C.W., Chen, C.K.: Bifurcation and chaos of a flexible rotor supported by turbulent journal bearings with non-linear suspension. Trans. IMechE Part J.: J. Eng. Tribol. **220**, 549–561 (2006)
14. Chang-Jian, C.W., Chen, C.K.: Nonlinear dynamic analysis of a flexible rotor supported by micropolar fluid film journal bearings. Int. J. Eng. Sci. **44**, 1050–1070 (2006)
15. Chang-Jian, C.W., Chen, C.K.: Bifurcation and chaos analysis of a flexible rotor supported by turbulent long journal bearings. Chaos Solitons Fractals **34**, 1160–1179 (2007)
16. Chang-Jian, C.W., Chen, C.K.: Nonlinear numerical analysis of a flexible rotor equipped with squeeze couple stress fluid film journal bearings. Acta Mech. Solida Sin. **20**(4), 283–290 (2007)
17. Chen, C.L., Yau, H.T.: Subharmonic and chaotic motion of a hybrid squeeze-film damper-mounted rigid rotor with active control. ASME J. Vib. Acoust. **124**, 198–208 (2002)
18. Li, Z.P., Luo, Y.G., Yao, H.L., Wen, B.C.: Nonlinear dynamic study of the elastic rotor-bearing systems with rub-impact fault. J. Northeast. Univ. (Nat. Sci.) **23**, 980–983 (2002)